Communications in Physics, Vol. 33, No. 3 (2023), pp. 273-284
DOI: https://doi.org/10.15625/0868-3166/18278

Effect of synthesis parameters on cobalt oxide nanostructures morphology

Hoang Thi Lan Anh[1,2], **Nguyen Minh Trung**[1,2], **Do Thi Kieu Anh**[1,2], **Dang Thi Thanh Le**[1,†], **Tran Vu Diem Ngoc**[2], **Do Thi Ngoc Tram**[3] **and Nguyen Duc Hoa**[1]

[1]*International Training Institute for Materials Science (ITIMS), Hanoi University of Science and Technology (HUST), No.1, Dai Co Viet Str., Hanoi, Vietnam*

[2]*School of Materials Science and Engineering (MSE), Hanoi University of Science and Technology (HUST), No.1, Dai Co Viet, Hanoi, Vietnam*

[3]*School of Engineering Physics (SEP), Hanoi University of Science and Technology (HUST), No.1, Dai Co Viet, Hanoi, Vietnam*

E-mail: †thanhle@itims.edu.vn; le.dangthithanh@hust.edu.vn

Received 18 April 2023
Accepted for publication 4 June 2023
Published 5 September 2023

Abstract. *A facile approach was employed for the synthesis of cobalt oxide nanorods (NRs) using cobalt nitrate, sodium oxalate and ethylene glycol as precursors via a hydrothermal process. The hydrothermal conditions, such as temperature and time, were varied to optimize the morphological characteristics of the NRs. After undergoing filtration, washing, and drying, the resulting material was characterized using several techniques, including scanning electron microscopy, energy-dispersive X-ray spectroscopy, X-ray diffraction, and transmission electron microscopy (TEM). Our findings reveal that the NRs exhibit diverse morphologies, depending on the hydrothermal conditions, with the smallest aspect ratio observed when prepared at 200˚C for 24 hours. In addition, we investigated the gas sensing capabilities of the NRs to ammonia under these conditions.*

Keywords: hydrothermal; nanorods; Co_3O_4; gas sensors.
Classification numbers: 61.46.Km; 07.07.Df.

1. Introduction

Cobalt oxide (Co_3O_4) is a significant transition metal oxide with magnetic and p-type semiconductor properties, exhibiting direct optical band gaps at 1.52 and 2.13 eV [1]. This compound has garnered significant attention for its potential applications in the fields of supercapacitors [2],

lithium-ion batteries [3, 4], and particularly gas sensors [5, 6]. Co_3O_4 belongs to the spinel-type metal oxide group, with the cubic phase being the most common crystal structure [7]. Various wet chemical methods have been employed to synthesize Co_3O_4 nanoparticles [8], nanocubes [9], nanosheets [10,11], nanotubes [12], nanowires [13], nanowalls [14], hollow polyhedrons [15], and hierarchical nanostructures [16–18].

Among the nanostructured Co_3O_4, one-dimensional (1D) nanostructures are considered to be the best morphology to improve gas sensing properties due to their high reaction surface and great miniaturization potential. Furthermore, 1D nanostructures are beneficial due to their unique advantages of a large length-to-diameter ratio and high charge carrier mobility.

Numerous research endeavors have been dedicated to the development of synthetic methodologies for the growth of cobalt oxide nanostructures, encompassing hydrothermal [19], electrospinning [20], chemical vapor deposition [1], sputtering [21] and pulsed laser deposition [22], among others. However, most of these deposition techniques entail demanding parameters such as high temperature, high vacuum, and complex reaction conditions, which ultimately lead to high production costs and impede widespread utilization of these materials. In comparison to other methods, the hydrothermal synthesis approach has garnered the most attention due to its facile operation and low power consumption, rendering it an attractive option for large-scale production of cobalt oxide nanostructures.

In this work, the obtained nanorods were synthesized via a hydrothermal process without surfactants. The first demonstration that porous Co_3O_4 nanorods can be prepared by an ethylene glycol-mediated process was published by our group in [23]. This study will investigate the morphological dependence of Co_3O_4 nanostructures on the time and temperature of the hydrothermal process.

2. Experiment

Ethylene glycol (EG) $(CH_2OH)_2$ ($\geq 99\%$), sodium oxalate $Na_2C_2O_4$ ($\geq 99.5\%$), and cobalt nitrate hexahydrate $Co(NO_3)_2 \cdot 6H_2O$ ($\geq 98\%$) were acquired from Sigma Aldrich (Germany) and utilized without additional purification.

The Co_3O_4 nanorods were created using a straightforward hydrothermal process. A common process involved dissolving cobalt nitrate and sodium oxalate in 50 ml of an ethylene glycol and water solution, followed by the addition of potassium oxalate. After vigorous stirring, a pale pink solution was produced. To guarantee that Co^{2+} ions were evenly distributed throughout the solution, two hours of nonstop magnetic stirring were used. After that, the solution was put into a 100 mL Teflon-lined stain-less steel autoclave. At diverse values of time of 3 h, 24 h and 48 h and temperatures of 120°C and 200°C, the autoclave was sealed and heated, the autoclave was heated following the heating procedure. The precipitated products were recovered by filtration, washing, and drying at 60°C. As a result, a powder product was obtained. Finally, the obtained materials were loaded into an alumina boat and inserted into a tubular furnace for calcination at 400°C for 2 h. The polycrystalline Co_3O_4 nanostructures were obtained by the calcination of this pink-green precursor, consisting in cobalt oxalate hydrate ($CoC_2O_4 \cdot 2H_2O$) short nanorods, at 400°C (Fig. 1).

The as-prepared material and the calcinated nanowires were characterized and analyzed by using X-ray diffraction (XRD), field emission scanning electron microscopy (FE-SEM), energy dispersive spectrometry (EDS) and high-resolution transmission electron microscopy (HRTEM).

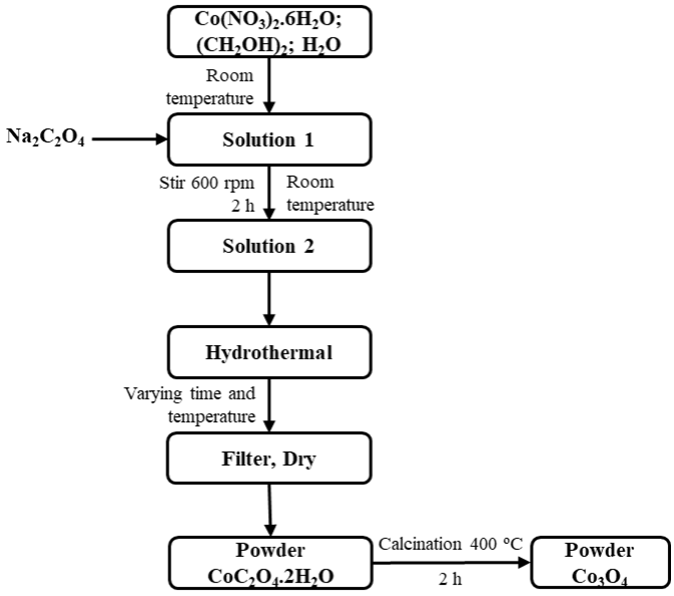

Fig. 1. Synthetic procedure of Co_3O_4 nanostructures at various times and temperatures.

The XRD analysis was performed using a Bruker D5005 X-ray diffractometer with CuKα1 radiation ($\lambda = 1.5406$ Å) at 40 kV and 40 mA. SEM images were obtained using a JEOL7600 scanning electron microscope at an accelerating voltage of 20 kV. Transmission electron microscopy (TEM) and electron diffraction images of the calcinated material were obtained using a JEOLJEM-2100 transmission electron microscope at an accelerating voltage of 200 kV.

The as-prepared material was uniformly coated onto interdigitated platinum electrode arrays that were deposited on silicon substrates to form a thick sensing film. The resulting sensor was annealed in air at 400˚C for 2 hours to enhance the stability of the material and improve adhesion between the material and the electrodes. The electrical resistance of the sensor was monitored using a Keithley 2602B source meter (Keithley, Solon, OH, USA) during cyclic exposure of NH_3 diluted in air (baseline gas) with the assistance of mass flow controllers (Kofloc, 3660, Korea) [24]. Pulses with analyte concentrations varying from 25 to 500 ppm were released, and the total gas flow was maintained at a constant rate of 400 sccm throughout the measurements.

The measurements were conducted using a home-built system, and the sensor's resistance was recorded at temperatures ranging from 200˚C to 350˚C, with steps of 50˚C. For a gas sensor based on p-type metal oxide semiconductor, the resistance of the device increases when exposed to reducing gases. The sensor response, denoted as $S=R_g/R_a$, where R_g and R_a represent the stable resistance of the device exposed to the target gas and air, respectively.

3. Rerults and discussion

3.1. Effect of synthesis time and temperature

The hydrothermal process was employed to regulate the morphology of the as-prepared cobalt oxalate nanostructures, with the time and temperature acting as the controlling factors.

SEM images of the cobalt oxalate nanorods synthesized at 120˚C for 3 hours, captured at various magnifications, are presented in Fig. 2. The images indicate that the obtained nanorods possess a diameter ranging from 300 to 500 nanometers, with lengths varying between 1 and 5 micrometers.

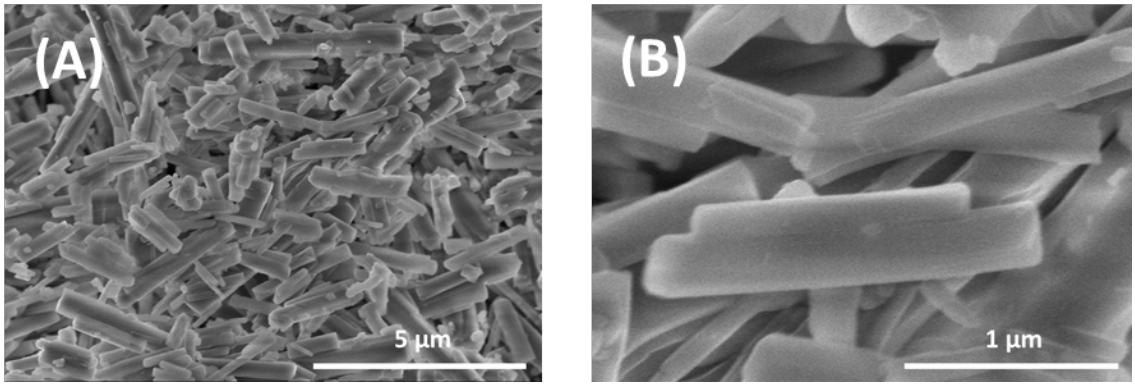

Fig. 2. SEM images of as-prepared cobalt oxalate nanostructure at 120˚C for 3 h at different magnifications: A) low magnification, B) high magnification.

Following the initial hydrothermal synthesis at 120˚C for 3 hours, the temperature was maintained, while the process time was extended up to 48 hours. The obtained product was characterized and displayed in Fig. 3, which shows SEM images of the cobalt oxalate nanorods captured at different magnifications. The images reveal that the diameter of the nanorods ranged from 500 to 700 nanometers, while the length varied from 2 to 5 micrometers. Notably, the nanorods' size increased, while their length remained relatively unchanged. Furthermore, the border of the nanorods appeared less distinct, and some of the nanorods appeared to merge.

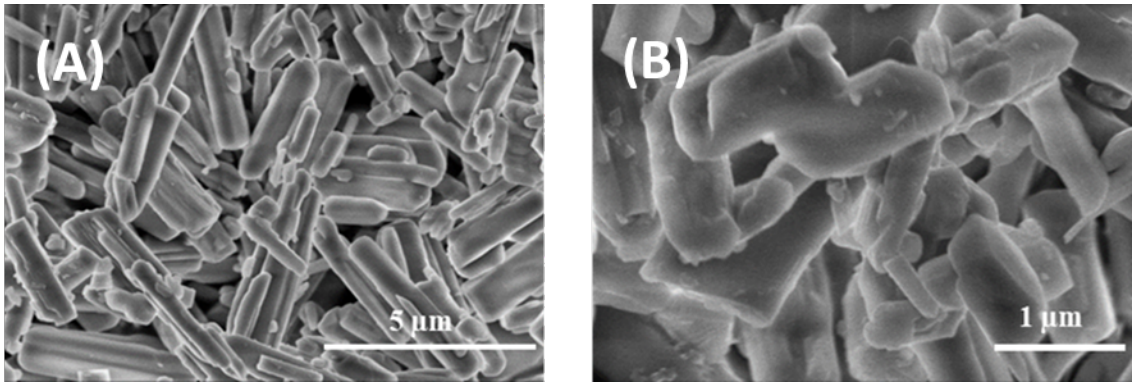

Fig. 3. SEM images of as-prepared cobalt oxalate nanostructure at 120˚C for 48 h at different magnifications: A) low magnification, B) high magnification.

To investigate the impact of the hydrothermal temperature on the morphology of the cobalt oxalate nanostructures, the hydrothermal time was held constant at 3 hours, while the process temperature was increased to 200˚C. The SEM images of the resulting cobalt oxalate nanostructures synthesized at 200˚C for 3 hours are displayed in Fig. 4.

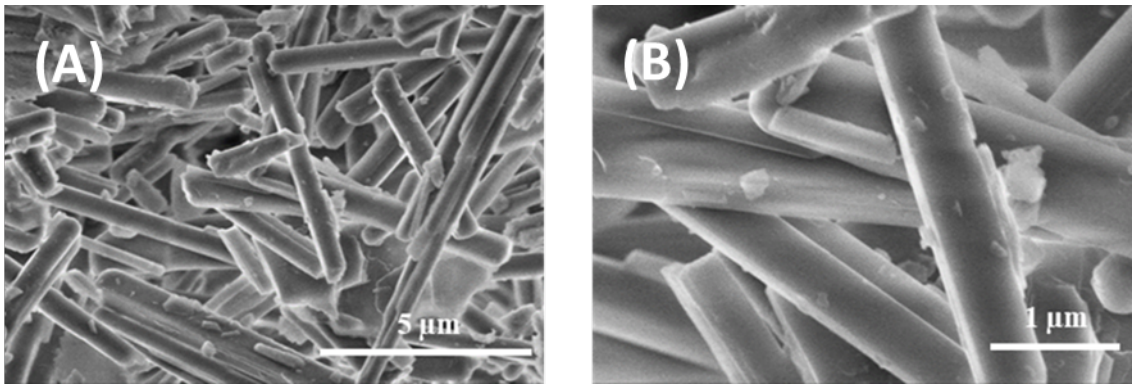

Fig. 4. SEM images of as-prepared cobalt oxalate nanostructure at 200˚C for 3 h at different magnifications: A) low magnification, B) high magnification.

It can be seen that the diameter of the nanorods ranged from 800 nm to 1 µm, while the length varied between 6 and 10 μm. This condition resulted in longer and wider nanorods in comparison to those prepared at 120˚C/3 h (Fig. 2).

Subsequently, the process temperature was maintained at 200˚C while the process time was extended to 24 hours. Under this condition, we obtained nanorods that were long in length but small in width, possessing a clear border. The SEM images of the synthesized nanorods captured at various magnifications are presented in Fig. 5. The obtained nanorods were uniform and smooth, with a diameter ranging from 500-800 nm and lengths varying between 10-20 μm.

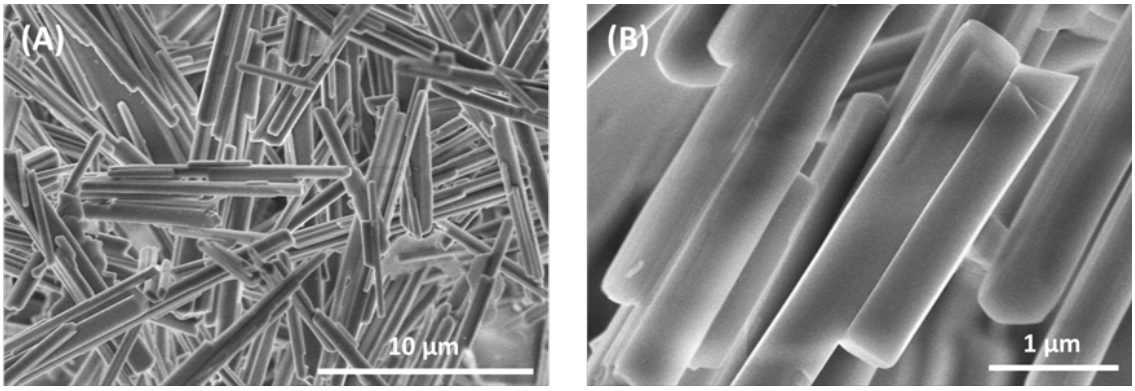

Fig. 5. SEM images of as-prepared cobalt oxalate nanostructure at 200˚C for 24 h at different magnifications: A) low magnification, B) high magnification.

Then time of the hydrothermal process were raised till 48 h while the temperature was still kept at 200˚C. At this condition of synthesis, morphology of nanorod was destroyed, as shown in Fig. 6. While at the same condition of time of 48 h, but at the condition of temperature of 120˚C, the morphology nanorod was still kept as shown in Fig. 3.

Therefore, after investigating effect of time and temperature of synthesis process on morphology of nanostructures, it is transparent to confirm that 200˚C/24 h is the best condition to

achieve smooth nanorods with small aspect ratio. This condition of synthesis was chosen for further characterizations in the current study.

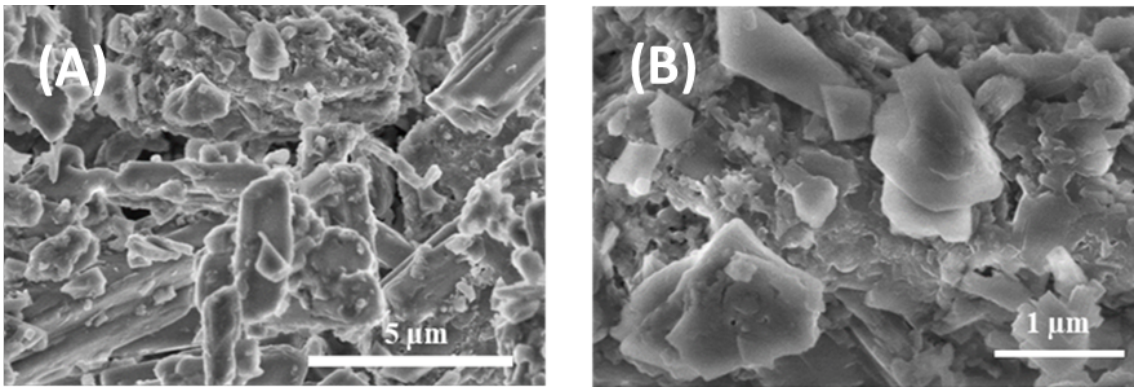

Fig. 6. SEM images of as-prepared cobalt oxalate nanostructure at 200˚C for 48 h at different magnifications: A) low magnification, B) high magnification.

3.2. Composition and Structural properties

The elemental composition of the sample was analyzed using EDS and EDS mapping techniques. The EDS elemental spectrum presented in Fig. 7a confirms the presence of cobalt (Co), carbon (C), and oxygen (O) elements in the as-prepared sample. Furthermore, the EDS mapping image (Fig. 7b) demonstrates that the distribution of Co, C, and O elements in the $CoC_2O_4 \cdot 2H_2O$ nanorods was uniform throughout the entire cobalt oxalate hydrate sample.

Figure 8 displays the X-ray diffraction (XRD) patterns of cobalt oxalate nanorods obtained after hydrothermal treatment at 200˚C for 24 h, as well as cobalt oxide nanorods after heat treatment at temperatures ranging from 300 to 700˚C for 2 h. The XRD pattern of the cobalt oxalate sample after hydrothermal treatment (represented by the black curve) displays four distinct diffraction peaks located at 2θ angles of 18.8°, 19.2°, 22.9°, and 30.4°. These peaks correspond to the (-202), (200), (002), and (-402) planes of the monoclinic structure of cobalt oxalate $CoC_2O_4 \cdot 2H_2O$, which is in agreement with the JCPDS spectrum library (tag 025-0251) for $CoC_2O_4 \cdot 2H_2O$. The XRD patterns of the Co_3O_4 samples after heat treatment at temperatures ranging from 300 to 700˚C display prominent diffraction peaks located at 2θ angles of 31.4°, 36.9°, 44.9°, 59.4°, and 65.3°. These peaks correspond to the (220), (311), (400), (511), and (440) planes of the cubic structure of Co_3O_4, which is in agreement with the JCPDS spectrum library (card 042-1467) for Co_3O_4. No additional diffraction peaks were detected, indicating the formation of a pure crystal structure. The (311) plane exhibited the highest intensity in all samples after heat treatment, indicating preferred growth in this direction. Moreover, the diffraction peak at 36.9° exhibited higher intensity compared to that of the Co_3O_4 sample after hydrothermal treatment, indicating the formation of Co_3O_4 crystals after heat treatment.

The sample morphology was characterized using FE-SEM and HRTEM, and the results are illustrated in Fig. 9, respectively. The image in Fig. 9a shows the morphology of the annealed Co_3O_4 porous nanorods, which are comprised solely of nanorods with an approximate diameter of 200-300 nm. No other morphologies were observed, indicating that the Co_3O_4 nanorods were

formed through the assembly of numerous nanoparticles. The SAED image (inset) confirms that the obtained Co_3O_4 nanorods are polycrystalline.

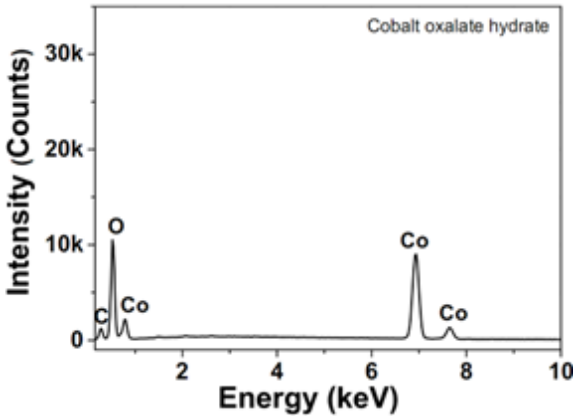

(a)

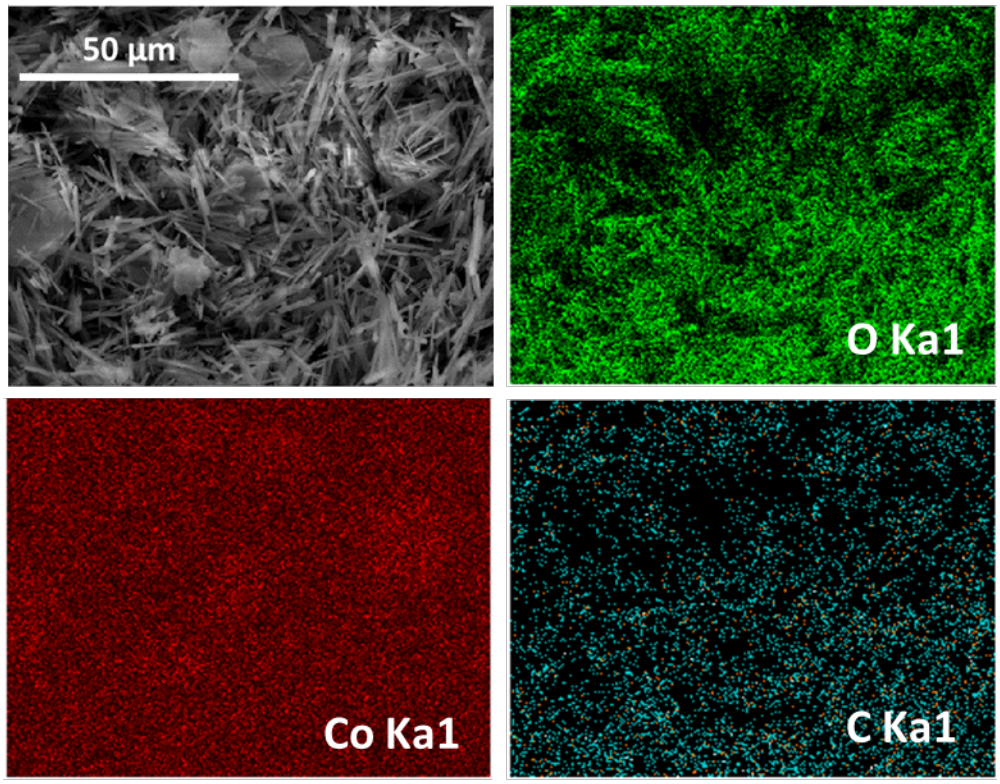

(b)

Fig. 7. a) EDS spectrum and b) EDS mapping of as-prepared cobalt oxalate nanorods at 200˚C for 24 h.

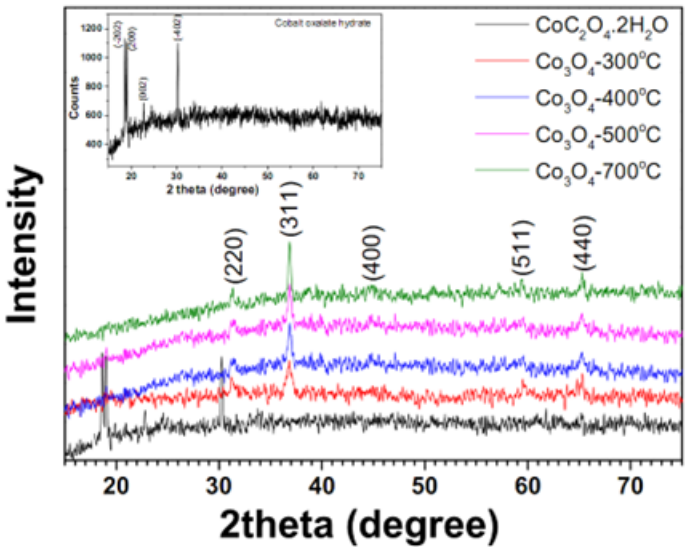

Fig. 8. XRD of as-prepared cobalt oxalate nanostructure at 200˚C/24 h and annealed at 300˚C; 400˚C; 500˚C; 700˚C. Inset: XRD of as-prepared cobalt oxalate nanostructure at 200˚C for 24 h.

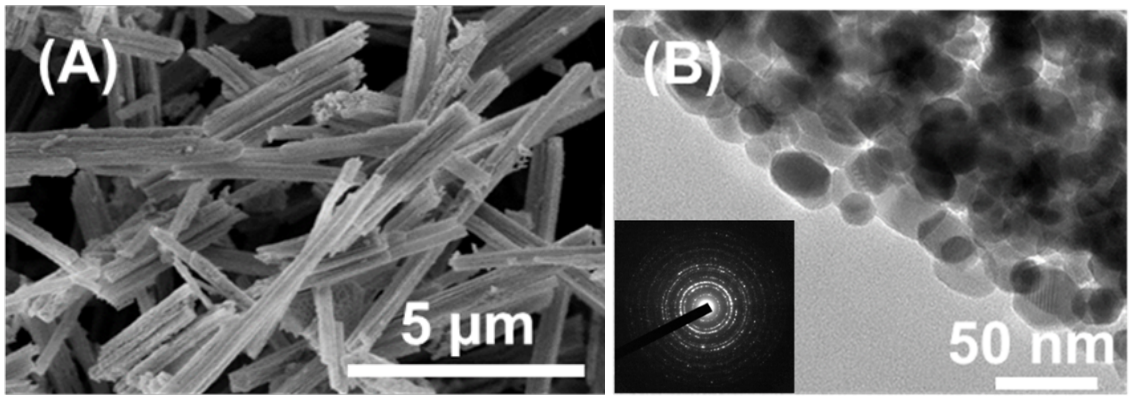

Fig. 9. A) FE-SEM image of the annealed Co_3O_4 polycrystalline nanorods, B) TEM image of the annealed Co_3O_4 polycrystalline nanorods. Inset: SAED image of the Co_3O_4 polycrystalline nanorods.

This finding is reinforced by the HRTEM image in Fig. 9b, which clearly illustrates the presence of nanoparticles with a width ranging from 10-30 nm, consistent with the SEM result. Together, these observations provide robust evidence that the synthesized Co_3O_4 nanorods possess a porous structure composed of interconnected nanoparticles.

3.3. Gas sensing property

The Co_3O_4 nanorods synthesized at 200˚C for 24 h then annealed at 400˚C for 2 hours were chosen to investigate ammonia sensing performance. The resistance change of a Co_3O_4 sensor

over time was examined at various operating temperatures (350, 300, 250, and 200˚C) and NH_3 gas concentrations (25, 50, 100, 250, and 500 ppm). The results, presented in Fig. 10, provide insight into the gas sensitivity of Co_3O_4 materials to NH_3 gas.

Figure 10a displays four real-time resistance change curves of the Co_3O_4 nanorod sensor at different operating temperatures. Upon exposure to NH_3 gas, the sensor's resistance increased and then returned to its original value upon removal of the gas source. This indicates the p-type semiconductor properties of the Co_3O_4 material. The gas sensing results reveal that the background resistance tends to increase with decreasing operating temperature. Specifically, at 350˚C, the background resistance reached approximately 360 Ω and increased to approximately 6250 Ω at 200˚C. At the operating temperature of 200˚C, the sample resistance did not recover to the background resistance after gas exposure.

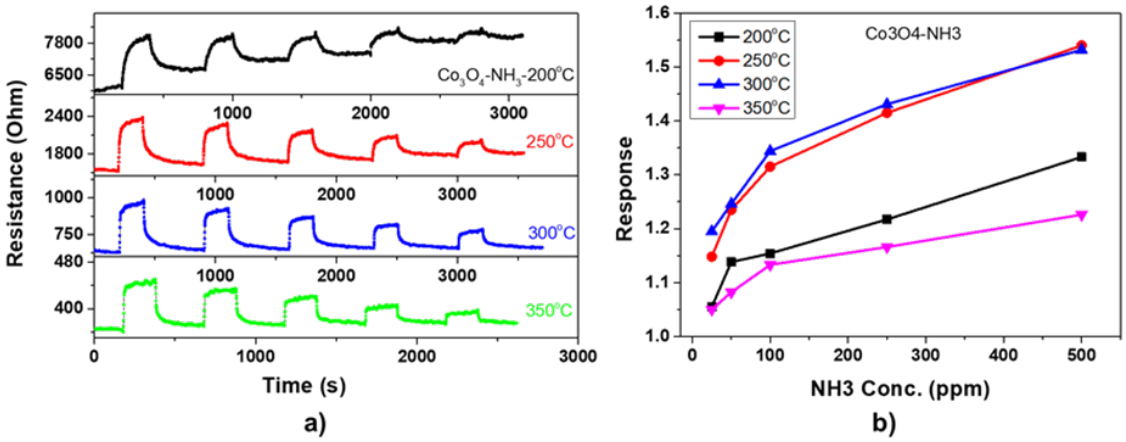

Fig. 10. Response to NH_3 of the Co_3O_4 sensor prepared at 200˚C/24 h: (a) Transient resistance verse response time to 25–500 ppm at various working temperatures 350˚C – 200˚C, (b) Response to diverse concentrations 25–500 ppm at different temperatures 350˚C – 200˚C.

Figure 10b displays the response calculated from Fig. 10a. The results indicate that at the operating temperature of 250˚C, the Co_3O_4 sensor exhibited the highest response to 500 ppm NH_3 gas (S=1.54 times). Conversely, when exposed to 100 ppm NH_3, the response of the material was only 1.13, 1.35, 1.31, and 1.15 at operating temperatures of 350, 300, 250, and 200˚C, respectively. The sensor's response increased with increasing gas concentration. In the low gas concentration range, the Co_3O_4 sensor exhibited a higher response at the operating temperature of 300˚C than at other operating temperatures. It is clear that the Co_3O_4 nanorod sensor exhibits the best performance at the operating temperature of 300˚C.

Co_3O_4 is a well-known p-type semiconductor, typically exhibiting this behavior under standard preparation conditions. However, upon exposure of Co_3O_4 nanorods to air, oxygen molecules tend to adsorb onto their surface, taking the form of O^- and O^{2-} ions. This can result in a high coverage of adsorbed oxygen ions that trap electrons within the nanostructure, ultimately increasing the number of charged holes and enhancing its conductivity in these conditions. When ammonia is introduced to the devices, its molecules react with the adsorbed oxygen, leading to the release

of the trapped electrons back into the nanorods layer. This process ultimately reduces the number of holes and results in a corresponding increase in sensor resistance.

Table 1. The comparison of ammonia sensing performance of Co_3O_4 nanomaterials in recent literature.

Material	**Method**	**T (˚C)**	**NH_3 conc. (ppm)**	**Response**	**Ref. (Year)**
Co_3O_4 nanofibers	Electrospinning	350	200	1.4	[25] (2023)
Co_3O_4/Ag_2O nanorods	Hydrothermal	90	20	No response	[26] (2022)
Co_3O_4 nanorods	Hydrothermal	200	20	No response	[27] (2021)
Co_3O_4/Cr nanorods	Hydrothermal	325	5	1.2	[28] (2014)
Co_3O_4 nanorods	**Hydrothermal**	**300**	**100**	**1.35**	**This work**

To evaluate the sensing capabilities of the Co_3O_4 nanorods we synthesized, we conducted a comparative analysis with prior research and compiled the results in Table 1. Our findings demonstrate that our fabricated sensor exhibits better performance in detecting NH_3 when compared to previously reported results.

4. Conclusion

This report discusses the hydrothermal synthesis of Co_3O_4 nanorods using ethylene glycol. The influence of synthesis time and temperature on the formation of $CoC_2O_4 \cdot 2H_2O$ nanorods was examined. The preparation condition at 200˚C for 24 hours gave the best cobalt oxide nanorods. Furthermore, the gas sensing properties of the synthesized Co_3O_4 nanorods towards NH_3 gas were studied. The sensor constructed using Co_3O_4 nanorods exhibited optimal response to NH_3 at the operating temperature of 300˚C.

Acknowledgement

This research is funded by Ministry of Education and Training under project number B2022-BKA-26 CTVL.

Authors contributions

Hoang Thi Lan Anh, Nguyen Minh Trung, Do Thi Kieu Anh: Investigation, Data curation. Tran Vu Diem Ngoc, Do Thi Ngoc Tram: Data curation, Formal analysis, Writing. Dang Thi Thanh Le: Methodology, Writing – review & editing, Supervision, Funding acquisition. Nguyen Duc Hoa: Writing – review & editing, Supervision.

Conflict of interest

The authors declare that there is no conflict of interest.

References

[1] A. Gulino, P. Dapporto, P. Rossi and I. Fragalà, *A Novel self-generating liquid MOCVD precursor for Co_3O_4 thin films*, Chem. Mater. **15** (2003) 3748.

[2] W. Guo, X. Lian, Y. Tian, T. Yang and S. Wang, *Facile fabrication 1D/2D/3D Co_3O_4 nanostructure in hydrothermal synthesis for enhanced supercapacitor performance*, J. Energy Storage **38** (2021) 102586.

[3] F. Zhan, B. Geng and Y. Guo, *Porous Co_3O_4 nanosheets with extraordinarily high discharge capacity for lithium batteries*, Chem. Eur. J. **15** (2009) 6169.

[4] Y. Ren, X. Xiao, J. Ni, H. Zhao, H. Yang and X. Chen, *RuO_2 incorporated Co_3O_4 nanosheets as carbon-free integrated cathodes for lithium-oxygen battery application*, Mater. Lett. **304** (2021) 130634.

[5] H. Nguyen, S.A. El-Safty, *Meso- and Macroporous Co_3O_4 Nanorods for Effective VOC Gas Sensors*, J. Phys. Chem. C. **115** (2011) 8466.

[6] P.L. Quang, N.D. Cuong, T.T. Hoa, H.T. Long, C.M. Hung, D.T.T. Le, N. Van Hieu, *Simple post-synthesis of mesoporous p-type Co_3O_4 nanochains for enhanced H_2S gas sensing performance*, Sens. Actuators B Chem. **270** (2018) 158.

[7] K. J. Kormondy, A. B. Posadas, A. Slepko, A. Dhamdhere, D. J. Smith, K. N. Mitchell, T. I. Willett-Gies *et al.*, *Epitaxy of polar semiconductor Co_3O_4 (110): Growth, structure, and characterization*, J. Appl. Phys. **115** (2014) 243708.

[8] P. G. Choi, T. Fuchigami, K. I. Kakimoto and Y. Masuda, *Effect of crystal defect on gas sensing properties of Co_3O_4 nanoparticles*, ACS Sens. **5** (2020) 1665.

[9] A. Ma, S. Y. Baek, J. H. Seo, S. A. Abbas, J.-H. Kwon, S. J. Ahn *et al.*, *Photodeposition of Pt Nanoparticles on Co_3O_4 nanocubes for detection of acetone at part-per-billion levels*, ACS Appl. Nano Mater. **4** (2021) 2752.

[10] H. Bazrafshan, R. S. Touba, Z. A. Tesieh, S. Dabirnia and B. Nasernejad, *Hydrothermal synthesis of Co_3O_4 nanosheets and its application in photoelectrochemical water splitting*, Chem. Eng. Commun. **204** (2017) 1105.

[11] J. Cao, S. Wang, X. Zhao, Y. Xing, J. Li and D. Li, *Facile synthesis and enhanced toluene gas sensing performances of Co_3O_4 hollow nanosheets*, Mater. Lett. **263** (2020) 127215.

[12] Z. Fei, S. He, L. Li, W. Ji, and C.-T. Au, *Morphology-directed synthesis of Co_3O_4 nanotubes based on modified Kirkendall effect and its application in CH4 combustion*, Chem. Commun. **48** (2012) 853.

[13] Y. Sun, P. Lv, J. Y. Yang, L. He, J. C. Nie, X. Liu *et al.*, *Ultrathin Co_3O_4 nanowires with high catalytic oxidation of CO*, Chem. Commun. **47** (2011) 11279.

[14] L. Xiong, Y. Teng, Y. Wu, J. Wang and Z. He, *Large-scale synthesis of aligned Co_3O_4 nanowalls on nickel foam and their electrochemical performance for Li-ion batteries*, Ceram. Int. **40** (2014) 15561.

[15] Y. Zhang, Y. Wu, Z. Duan, B. Liu, Q. Zhao, Z. Yuan *et al.*, *High performance humidity sensor based on 3D mesoporous Co_3O_4 hollow polyhedron for multifunctional applications*, Appl. Surf. Sci. **585** (2022) 152698.

[16] J. Cao, S. Wang, J. Li, Y. Xing, X. Zhao and D. Li, *Porous nanosheets assembled Co_3O_4 hierarchical architectures for enhanced BTX (benzene, toluene and xylene) gas detection*, Sens. Actuators B Chem. **315** (2020) 128120.

[17] Z. Zhang, Y. Song and J. Sun, *Self-stacked $Co(OH)_2/Co_3O_4$ nanosheets for high-selectivity gas sensor to n-butyl alcohol*, Appl. Surf. Sci. **610** (2023) 155438.

[18] J. Deng, R. Zhang, L. Wang, Z. Lou and T. Zhang, *Enhanced sensing performance of the Co_3O_4 hierarchical nanorods to NH_3 gas*, Sens. Actuators B Chem. **209** (2015) 449.

[19] Y. Qiu, Y. Wang, *Controllable synthesis of porous Co_3O_4 nanorods and their ethanol-sensing performance*, Ceram. Int. (2022).

[20] P. H. Phuoc, L. T. Hong, N. T. Thang, N. H. Hanh, C. M. Hung, N. V. Duy *et al.*, *Fabrication of p-type Co_3O_4 nanofiber sensors for ultra-low H_2S gas detection at low temperature*, J. Nanosci. Nanotechnol. **21** (2021) 2626.

[21] R. Hippler, M. Cada, P. Ksirova, J. Olejnicek, P. Jiricek, J. Houdkova *et al.*, *Deposition of cobalt oxide films by reactive pulsed magnetron sputtering*, Surf. Coatings Technol. **405** (2021) 126590.

[22] H. Y. Kwong and Y. W. Wong, *Formation of cobalt hydroxide single-crystal platelets from pulsed laser deposited cobalt thin film*, J. Alloys Compd. **497** (2010) 267.

[23] N.M. Le, H.L. Nguyen, T.T. Le Dang, T. Matteo, V.D.N. Tran, H.M. Luu, T.H.D. Truong, D.H. Nguyen, *Synthesis of cobalt oxide nanorods using hydrothermal method*, 5th Int. Conf. Adv. Mater. Nanotechnology, Nov 16-19. Hanoi (2022) 207

[24] L. Van Duy, T.T. Nguyet, D.T.T. Le, N. Van Duy, H. Nguyen, F. Biasioli, M. Tonezzer, C. Di Natale, N.D. Hoa, *Room Temperature Ammonia Gas Sensor Based on p-Type-like V_2O_5 Nanosheets towards food spoilage monitoring*, Nanomaterials. **13** (2022) 146.

[25] P. H. Phuoc, N. N. Viet, N. V. Chien, N. V. Hoang, C. M. Hung, N. D. Hoa *et al.*, *Comparative study of CuO/Co_3O_4 external and CuO-Co_3O_4 internal heterojunctions: Do these factors always enhance gas-sensing performance?*, Sens. Actuators B Chem. **384** (2023) 133620.

[26] G. Lei, C. Lou, Z. Li, J. Xie, G. Lu, H. Pan *et al. Heterogeneous Co_3O_4/Ag_2O nanorods for conductometric triethylamine sensing at 90˚C*, Sens. Actuators B Chem. **351** (2022) 131005.

[27] X. Qiao, C. Ma, X. Chang, X. Li, K. Li, L. Zhu *et al.*, *3D radial Co_3O_4 nanorod cluster derived from cobalt-based layered hydroxide metal salt for enhanced trace acetone detection*, Sens. Actuators B Chem. **327** (2021) 128926.

[28] H. M. Jeong, H. J. Kim, P. Rai, J. W. Yoon and J. H. Lee, *Cr-doped Co_3O_4 nanorods as chemiresistor for ultraselective monitoring of methyl benzene*, Sens. Actuators B Chem. **201** (2014) 482.